
OP2GS: Object-Aware 3D Gaussian Primitives via Dual Opacity

Guiyu Liu¹ Niklas Vaara¹ Janne Mustaniemi¹ Juho Kannala^{1,2}
Janne Heikkilä¹

¹Center for Machine Vision and Signal Analysis, University of Oulu, Finland

²Aalto University, Finland

Abstract

3D Gaussian Splatting (3DGS) provides an explicit and efficient scene representation, but its primitives lack inherent object-level identity, hindering downstream tasks such as open-vocabulary scene understanding. Existing methods typically address this by either distilling high-dimensional feature embeddings into Gaussians or by lifting 2D mask labels into 3D via heuristic refinement. However, feature-based approaches incur heavy storage and decoding overhead, while lifting-based pipelines remain vulnerable to label contamination: Gaussians necessary for appearance reconstruction often receive incorrect object labels during 2D-to-3D projection.

We propose *OP2GS*, an object-aware Gaussian representation that augments each primitive with an explicit instance identity and a dedicated instance opacity σ^* for object-mask rendering. The original opacity σ remains responsible for visual reconstruction, while σ^* models whether a Gaussian should contribute to a particular object mask. This dual-opacity formulation decouples visual existence from instance occupancy: mislabeled Gaussians can remain available for image rendering while becoming transparent in the object-mask branch.

To learn this representation, we introduce a random object loss that optimizes the 1D instance occupancy field using the standard transmittance-based visibility of 3DGS. Semantic descriptors are then attached at the object level through multi-view aggregation, eliminating per-Gaussian feature storage. Compared with feature-training approaches, OP2GS achieves competitive open-vocabulary performance while significantly reducing computational overhead. Compared with training-free pipelines, it leverages physically consistent occupancy learning to resolve visibility ambiguities. Experiments on open-vocabulary benchmarks demonstrate that OP2GS provides a compact and robust object-aware representation with a superior balance of accuracy and efficiency.

1 Introduction

Open-vocabulary 3D scene understanding provides a natural testbed for evaluating whether a 3D representation can support object-level reasoning beyond image synthesis. 3D Gaussian Splatting (3DGS) [2] has emerged as an efficient explicit representation for real-world scenes, yet its primitives are primarily defined by geometry, color, and opacity, without an explicit notion of object identity. As a result, existing 3DGS-based methods typically introduce object-level information through feature rendering or mask lifting. Feature-based methods attach semantic or instance embeddings to Gaussians and recover object labels through rendering and decoding [3–5]. Beyond computational overhead, feature fields may exhibit cross-view inconsistency after alpha compositing; our dual-opacity formulation instead exploits the inherent view-consistency of 3DGS opacity as a stable scalar signal for mask rendering.

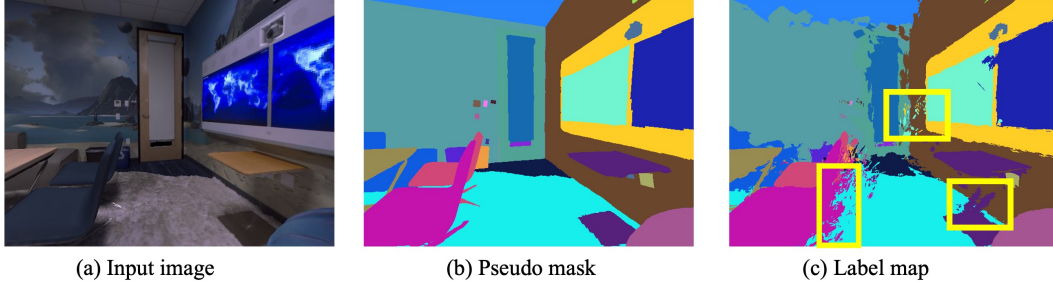


Figure 1: Label contamination in hard mask lifting. (a) Input image. (b) SAM [1] mask as pseudo label for lifting labels. (c) Label map rendered after majority-voting lifting with depth culling by selecting the Gaussian with the largest $\alpha_i T_i$ (rendering weight) along each ray. One of the yellow boxes shows floater Gaussians incorrectly assigned to the "chair" instance. This occurs because the dominant Gaussian along a ray is not always located near the object surface. In particular, in dark regions where the overall opacity is low, floater Gaussians can easily have the largest rendering weight.

Lifting-based methods(e.g., [6–8]) project 2D masks into the Gaussian field and then refine the resulting assignments through majority voting, rendering weight filtering, clustering, or additional optimization. A central difficulty in lifting 2D masks to 3DGS is label contamination. Since 3DGS uses soft, semi-transparent primitives and alpha compositing, a 2D foreground mask does not always correspond cleanly to a single set of foreground Gaussians. Inaccurate depth estimation, boundary ambiguity, or floater Gaussians from densification may be assigned to an object because they project into the same masked region, even though they should not contribute to that object’s segmentation. As shown in Fig. 1, floater Gaussians can have dominant rendering weight. Once an incorrect identity is attached, the representation lacks a separate mechanism to suppress that Gaussian in object-mask rendering without also affecting its role in appearance reconstruction.

We argue that this limitation arises from using a single opacity field to serve two different purposes. The original 3DGS opacity σ is an appearance-oriented property. For object-level scene understanding, however, we also need an instance occupancy property: whether the Gaussian should contribute to a particular object mask. These two notions are not equivalent.

To address this, we propose *OP2GS*, an object-aware Gaussian representation with dual opacity. In addition to the original radiance opacity σ , each Gaussian is equipped with an instance opacity σ^* , which acts as a 1D instance occupancy field for object-mask rendering. This design decouples visual appearance from instance occupancy. A mislabeled Gaussian can remain visually present through σ to preserve the reconstructed scene, while becoming transparent in the object-mask branch through a low σ^* so that it no longer contaminates the object mask. In this sense, OP2GS is not merely adding another scalar parameter; it redefines the Gaussian primitive as an object-aware entity whose mask contribution can be optimized independently from its appearance contribution.

We design a random object loss to learn this instance occupancy field by improving the instance opacity of Gaussians that belong to the specific object in each iteration. The instance opacity rendering branch reuses the original 3DGS transmittance and early termination: once the accumulated transmittance becomes negligible, occluded Gaussians behind the ray are skipped, while mislabeled Gaussians that cause false positives are suppressed by lowering their instance opacity.

After learning object-aware Gaussians, we get the object-level feature through multi-view object feature aggregation, enabling open-vocabulary queries without storing features for every Gaussian. We evaluate OP2GS using open-vocabulary segmentation as a representative downstream task, where object identity, vision-language feature attachment, and rendered masks can be measured directly. Our goal is to show that a compact object-aware Gaussian representation can support efficient open-vocabulary scene understanding while addressing label contamination in direct mask lifting.

Our main contributions are:

- **Dual-opacity representation.** We augment each Gaussian with an instance opacity σ^* , decoupling visual reconstruction from object-mask rendering.

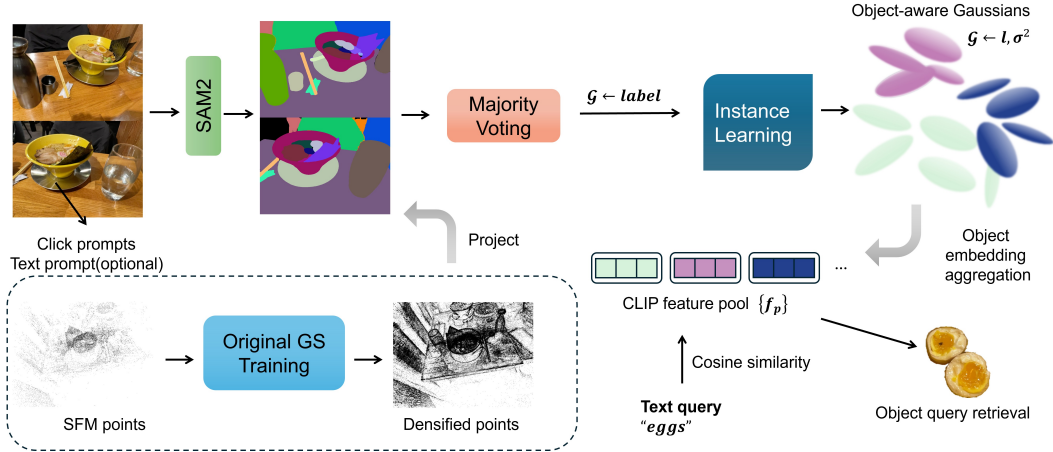


Figure 2: The overall pipeline of our proposed *OP2GS*

- **Visibility-aware instance learning.** We optimize σ^* with a random object loss that reuses 3DGS transmittance, suppressing label contamination from floaters and ambiguous mask lifting.
- **Compact open-vocabulary segmentation.** *OP2GS* avoids high-dimensional per-Gaussian feature rendering while achieving competitive accuracy and 121 FPS inference.

2 Related work

2.1 3D Gaussian Splatting based Representation

3D Gaussian Splatting (3DGS) [2] represents a scene with anisotropic Gaussian primitives and renders images through differentiable alpha compositing. Scaffold-GS [9], further improve densification control and training stability. Beyond novel-view synthesis, many works extend 3DGS with additional semantic or instance-level representations. Feature 3DGS [3] distills 2D foundation-model features (CLIP [10]) into Gaussian feature fields for segmentation. SAGA [11] learns scale-gated affinity features to support multi-granularity 3D segmentation. For instance-level reasoning, Gaussian Grouping [4] introduces compact identity encodings supervised by multi-view SAM masks and 3D spatial regularization, while ObjectGS [12] optimizes rendered one-hot object labels with Scaffold-GS-based densification control. These methods show that object-level reasoning benefits from semantic or instance augmentation, but most require rendering and optimizing multi-dimensional feature or label fields, increasing memory and rendering overhead and potentially causing feature inconsistency after alpha compositing. In contrast, *OP2GS* keeps the standard 3DGS representation and densification strategy while augmenting each primitive with only a scalar instance opacity and an integer label.

2.2 Open-vocabulary 3D Scene Understanding

Early methods such as LERF [13] and OpenNeRF [14] embed CLIP features into NeRF volumes, while per-scene 3DGS methods such as LangSplat [15] and OpenGaussian [5] learn explicit language-aware Gaussian features. Feed-forward approaches such as SceneSplat [16] further aim to predict semantic or language-aligned Gaussian features for unseen scenes. Nevertheless, efficient and compact per-scene object-level representations remain useful for edge devices and interactive applications, where rendering cost and memory footprint are critical. This motivates representations that preserve object-level accessibility while avoiding dense per-Gaussian feature decoding. For instance-level reasoning, methods such as Click-Gaussian [17], Gaussian Grouping [4], ObjectGS [12], and ILGS [18] optimize object-aware embeddings or labels for open-vocabulary segmentation and interaction. Meanwhile, training-free approaches [6–8, 19, 20] directly lift or associate 2D visual features with 3D primitives. LightSplat [6] attaches each Gaussian with a compact 2-byte cluster index, but still relies on scene-dependent thresholds and rendering-weight-based associations. LUDVIG [20] directly

lifts 2D features to 3D Gaussians using the original rendering weights, but the semantic assignment remains coupled with the radiance opacity optimized for photometric reconstruction.

However, these methods often depend on photometric rendering weights or heuristic feature associations, making label assignments sensitive to boundary ambiguity, floaters, and challenging appearance effects such as transparency and reflections. In contrast, OP2GS introduces a dedicated instance opacity decoupled from radiance rendering, enabling more stable object occupancy modeling.

3 Method

3.1 OP2GS Representation

3D Gaussian Splatting representation. In the standard 3D Gaussian Splatting framework [2], a scene is represented by a collection of n 3D Gaussian primitives \mathcal{G} . Each Gaussian is characterized by its center position μ , color c (spherical harmonics coefficients), opacity σ , rotation R (quaternion), and scale S . These Gaussians are projected onto the image plane through differentiable rasterization \mathcal{D} to generate a rendered image I_{ren} from a given viewpoint. The model is trained by minimizing the reconstruction loss \mathcal{L}_{rgb} between the rendered image I_{ren} and the ground-truth image I_{gt} . This pipeline can be summarized as follows, where parameters shown in blue are optimizable:

$$\mathcal{G}(\mu, c, \sigma, R, S)_n \xrightarrow{\mathcal{D}} I_{ren} \longrightarrow \mathcal{L}_{rgb} \longleftarrow I_{gt} \quad (1)$$

OP2GS representation. Our method extends the original representation with an additional instance opacity σ^* and a scalar label l , where σ^* serves as a 1D instance occupancy field for object-mask rendering. Rather than previous methods [3–5] that use a high-dimensional feature f to encode identity, we use a scalar occupancy value σ^* together with an integer label l , making object-mask rendering efficient.

$$\mathcal{G}(\mu, c, \sigma, R, S, \sigma^*, l)_n \xrightarrow{\mathcal{D}} S(v), I_{ren} \longrightarrow \mathcal{L}_{rgb}, \mathcal{L}_{obj} \longleftarrow B, I_{gt} \quad (2)$$

where $S(v)$ denotes the instance occupancy map(detailed in Sec. 3.3.1), while B is the binary pseudo-label mask for the objects.

3.2 Initialization

OP2GS is trained in two stages. We first train a standard 3DGS model until densification stabilizes, and then initialize each Gaussian with a scalar object label l before optimizing the additional instance opacity σ^* in the second stage.

To obtain l , we generate view-consistent instance masks using off-the-shelf SAM2, project each Gaussian center μ_j onto the training views, and assign its label by majority voting over the projected mask IDs. This keeps the original densification and pruning strategy unchanged while avoiding high-dimensional identity features or one-hot encodings. Details of SAM2 pseudo-label generation, the comparison with SAM+DEVA, and the voting strategy are provided in the appendix.

3.3 Instance Learning

In the second stage, when the original opacity parameter σ is about to converge, we introduce the additional instance opacity σ^* and start optimizing it using the proposed random object loss \mathcal{L}_{obj} .

3.3.1 Object-specific Opacity Rendering

In the original 3D Gaussian Splatting framework [2], the rendering result for pixel v is defined as:

$$C(v) = \sum_{i \in \mathcal{N}} c_i \alpha_i T_i, \quad (3)$$

where \mathcal{N} represents the ordered Gaussians along the ray, c_i is the color of the i -th Gaussian, and $\alpha_i = \sigma_i G_i^{2D}(v)$, with σ_i denoting the original opacity and $G_i^{2D}(\cdot)$ the projected 2D Gaussian distribution of the i -th 3D Gaussian. T_i denotes the transmittance.

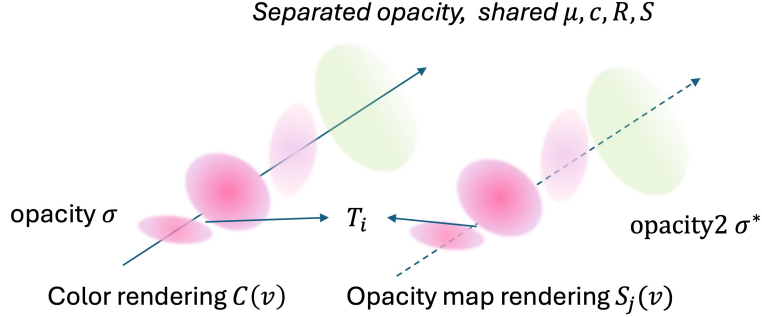


Figure 3: Illustration of the dual-opacity rendering process. The dashed line indicates the same ray direction used for both color and opacity rendering.

To enable object-level reasoning, we introduce an instance occupancy field parameterized by σ^* . For object j , its rendered instance occupancy map $S_j(v)$ represents the accumulated object occupancy at pixel v . The rendering of $S_j(v)$ follows the standard alpha-blending process:

$$S_j(v) = \sum_{i \in \mathcal{O}_j} \alpha_i^* T_i, \quad (4)$$

where \mathcal{O}_j denotes the set of Gaussians belonging to object j , and $\alpha_i^* = \sigma_i^* G_i^{2D}(v)$ denotes the object-specific opacity contribution of Gaussian i at pixel v .

As shown in Fig. 3, we use the same transmittance T_i as in Eq. (3). The 2D Gaussian distribution $G_i^{2D}(v)$ is also shared with the original color rendering. Only σ_i^* is newly introduced as a trainable parameter, while the Gaussian’s position μ , color c , rotation R , and scaling S remain shared across both rendering branches.

3.3.2 Random Object Loss

After obtaining the instance occupancy map $S_j(v)$, we design a random object loss to learn the instance occupancy field σ^* :

$$\mathcal{L}_{\text{obj},j} = L_{\text{CE}}(S_j(v), B_j) \quad (5)$$

where B_j denotes the pseudo-label binary mask for object j , and L_{CE} represents the cross-entropy loss. “Random” refers to randomly sampling a subset of instance IDs per iteration to update their σ^* values, which reduces computation while still covering all objects over training. For object j , $B_j = 1$ indicates pixels that belong to object j , and $B_j = 0$ otherwise. Since the maximum accumulated occupancy is 1, we use the binary mask to supervise $S_j(v)$ as an object occupancy map.

During initialization, the projection and majority-voting strategies may still assign incorrect labels to some Gaussian points. Because $S_j(v)$ represents the accumulated instance opacity of object j at pixel v , this loss encourages the instance opacity of correctly labeled objects to increase. Meanwhile, the σ^* values of mislabelled Gaussians are suppressed toward zero, leading these points to be effectively removed during training.

As each training image contains multiple objects, rendering all of them simultaneously would be computationally expensive. Therefore, we randomly sample M objects at each training step and average their losses:

$$\mathcal{L}_{\text{obj}} = \frac{1}{M} \sum_{j=1}^M \mathcal{L}_{\text{obj},j} \quad (6)$$

where M is the number of randomly sampled objects (we set $M = 3$ in our experiments). After several thousand training steps, all objects are iteratively optimized, and the σ^* values of incorrectly labeled Gaussians are suppressed close to zero.

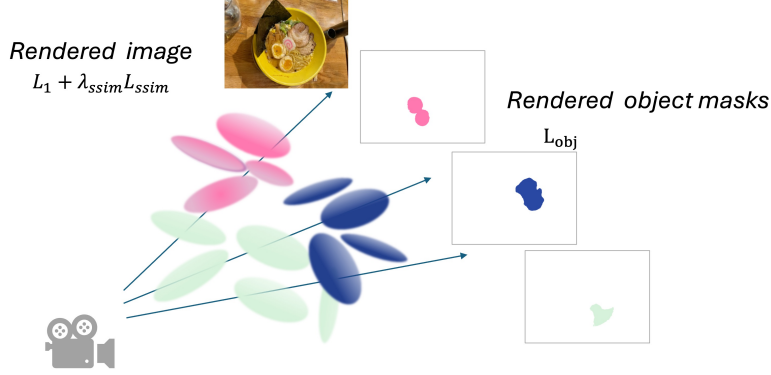


Figure 4: Visualization of the training objective: different colors indicate Gaussians with various initial labels. Gaussians associated with the three objects are selected for random object loss. All Gaussians still contribute to the appearance loss of rendered images as before.

3.3.3 The Backward Path

During the second stage, the gradients from both \mathcal{L}_{rgb} and \mathcal{L}_{obj} are backpropagated to update the parameters of the Gaussians.

Loss-specific gradient paths Importantly, the two losses have different gradient paths:

- \mathcal{L}_{rgb} updates: σ_i (original opacity), c_i (color), and geometric parameters μ_i, R_i, S_i (via $G_i^{2D}(v)$).
- \mathcal{L}_{obj} updates: σ_i^* (instance opacity) and geometric parameters μ_i, R_i, S_i (via $G_i^{2D}(v)$).

This design allows independent optimization of appearance (σ_i, c_i) and instance (σ_i^*), while both losses collaborate to refine geometry (μ_i, R_i, S_i). For the newly introduced parameter σ_i^* , the gradient is computed as:

$$\frac{\partial \mathcal{L}_{obj}}{\partial \sigma_i^*} = \frac{\partial \mathcal{L}_{obj}}{\partial S_j(v)} \cdot T_i \cdot G_i^{2D}(v), \quad (7)$$

The gradient stops at T_i , where the gradient flows through the instance map $S_j(v)$ but does not affect the original opacity σ_i or color c_i .

Both losses share and optimize the geometric parameters through the 2D Gaussian distribution $G_i^{2D}(v)$, where L is from Eq. 9

$$\frac{\partial \mathcal{L}}{\partial G_i^{2D}(v)} = \frac{\partial \mathcal{L}}{\partial \alpha_i} \cdot \sigma_i + \frac{\partial \mathcal{L}}{\partial \alpha_i^*} \cdot \sigma_i^* \quad (8)$$

3.4 Training Objective

With the help of the alpha rendering, our method can jointly optimize the two objectives. As seen in Fig. 4, our overall training loss for the second stage is:

$$\mathcal{L} = \mathcal{L}_1 + \lambda_{SSIM} \mathcal{L}_{SSIM} + \lambda_o \mathcal{L}_{obj}, \quad (9)$$

where \mathcal{L}_1 and \mathcal{L}_{SSIM} are the L_1 and $SSIM$ loss between rendered images and ground-truth images, and \mathcal{L}_{obj} is the proposed random object loss. λ_o is the weight for the object loss. λ_{SSIM} comes from the original 3DGS training objective.

3.5 Open-Vocabulary Segmentation

The labels in our method are fixed integer IDs assigned during initialization (Section 3.2). The proposed random object loss suppresses the mislabeled Gaussians while adaptively refining their spatial shapes. After optimization, the refined Gaussians and stable labels allow rendering of consistent object masks from arbitrary viewpoints.

3.5.1 Object Embedding Aggregation

Instead of rendering dense language features, we first convert the learned instance occupancy field into object-level geometry gates. For object j in view i , we threshold the rendered instance occupancy map $S_j^i(v)$ to obtain a binary mask:

$$M_j^i = \mathbf{1} [S_j^i(v) > \tau], \quad \tau = 0.5. \quad (10)$$

Here, $S_j^i(v)$ is produced by the instance-opacity branch and encodes whether the visible Gaussians along each ray belong to object j . The thresholded mask therefore acts as a geometry gate that selects the visible object region before feature extraction, rather than mixing features through α -blending.

We then compute an object embedding by averaging CLIP features from the gated object crops across N selected views:

$$f_j = \frac{1}{N} \sum_{i=1}^N \text{CLIP}(\mathcal{C}(M_j^i \otimes I_i)), \quad (11)$$

where $\mathcal{C}(\cdot)$ denotes crop-and-resize, $M_j^i \otimes I_i$ is the masked image region, and $N = 5$ in our experiments. This object-level aggregation produces one semantic descriptor per object, making open-vocabulary querying independent of per-Gaussian feature rendering or decoding.

3.5.2 Open-Vocabulary Query

After obtaining the object embeddings $\{f_p\}$ for all objects in the scene (Section 3.5.1), we construct an object feature pool of all objects in the scene. Given an input text prompt, we perform open-vocabulary querying using the standard argmax operation over cosine similarities between the query embedding and the object embeddings, following [15, 18, 21]. The visualization process is shown in appendix.

3.6 Instance Segmentation

Although our method is primarily designed for open-vocabulary segmentation, it also enables fast and lightweight instance segmentation using the proposed additional σ^* without additional supervision. For each ray, the Gaussian with the largest σ^* value is considered to contribute the most to the corresponding pixel. The instance label of that pixel is then assigned as the label associated with this dominant Gaussian:

$$I(v) = \ell_{\arg, \max_{i=1, \dots, N} \alpha_i^*(v)} \quad (12)$$

where ℓ denotes the label attached to each Gaussian point, and N is the number of Gaussians intersected by the ray before being terminated by the accumulated transmittance T_i .

4 Experiment

4.1 Setting and Datasets

To assess the segmentation performance of our proposed method, we conduct experiments on two open-vocabulary scene datasets: the 3DOVS dataset [22] and the LERF-mask dataset [13]. We follow the Gaussian Grouping approach [4] to evaluate our method. For the Replica dataset [23], we perform qualitative evaluations for instance segmentation. The implementation details are described in the appendix.

4.2 Open-Vocabulary Segmentation

Comparison with state-of-the-art methods. We evaluate our method on two widely used benchmarks for open-vocabulary 3D segmentation: 3DOVS [22] and LERF-Mask [13]. The quantitative results on the 3DOVS dataset are shown in Tab. 1. Our method achieves the mean mIoU of 97.1% on 3DOVS, surpassing the previous best result of ObjectGS [12]. Results for the remaining five scenes in 3DOVS dataset are reported in the appendix. On the LERF-Mask dataset (Tab. 2), our approach outperforms prior methods on two out of three scenes, achieving mIoU scores of 92.3% on *figurines* and 91.0% on *ramen*. These results validate the effectiveness of our dual-opacity design and random object loss for open-vocabulary 3D segmentation.

Table 1: Open-vocabulary 3D segmentation results. We report mIoU (%) on 3DOVS dataset following prior work.

Method	bed	bench	room	lawn	sofa	MEAN
LSEG [24]	56.0	6.0	19.2	4.5	17.5	20.6
OVSeg [25]	79.8	88.9	71.4	66.1	81.2	77.5
LERF [13]	73.5	53.2	46.6	27.0	73.7	54.8
3DOVS [22]	89.5	89.3	92.8	74.0	88.2	86.8
LangSplat [15]	77.8	77.3	58.4	90.9	60.2	73.0
Gaussian Grouping [4]	64.5	95.6	96.4	97.0	91.3	89.1
SAGA [11]	97.4	95.4	96.8	96.6	93.5	96.0
LBG [26]	97.7	96.3	95.9	97.3	87.4	94.9
ILGS [18]	96.4	95.5	93.6	92.2	94.2	94.4
ObjectGS [12]	98.0	96.4	95.1	97.2	95.4	96.4
Ours	97.5	96.3	97.4	97.7	96.4	97.1

Table 2: Open-vocabulary segmentation results on the LERF-Mask dataset. We follow Gaussian Grouping [4] to evaluate the method.

Model	figurines		ramen		teatime	
	mIoU	mBIoU	mIoU	mBIoU	mIoU	mBIoU
DEVA [27]	46.2	45.1	56.8	51.1	54.3	52.2
LERF [13]	33.5	30.6	28.3	14.7	49.7	42.6
SA3D [28]	24.9	23.8	7.4	7.0	42.5	39.2
LangSplat [15]	52.8	50.5	50.4	44.7	69.5	65.6
Gaussian Grouping [4]	69.7	67.9	77.0	68.7	71.7	66.1
Gaga [11]	90.7	89.0	64.1	61.6	69.3	66.0
ILGS [18]	75.9	73.8	84.3	75.5	81.2	78.8
ObjectGS [12]	88.2	85.2	88.0	79.9	88.9	88.6
Ours	92.3	89.1	91.0	84.6	87.0	85.4

Runtime analysis. To assess the speed improvement of our method, we compare the inference runtime breakdown with previous methods on the LERF-Mask scene *figurines*. Since ObjectGS is based on the Scaffold-GS [9] framework, it produces more points during densification. To ensure a fair comparison, all methods are evaluated with the same number of Gaussian points (1.6 million), and the average runtime is measured over 100 frames. Note that ObjectGS [12] uses variable feature dimensions for different scenes; for the LERF-Mask dataset, we re-implement ObjectGS in the same framework as Gaussian Grouping with 32-dimensional features. As shown in Tab. 3, our method achieves the fastest inference speed (121.7 FPS), significantly outperforming Gaussian Grouping and ObjectGS. This efficiency is primarily due to our compact parameter design (2D per Gaussian), which also reduces memory usage. Although LangSplat [15] uses 3-dimensional features, it still requires a decoder to map the feature to CLIP space, and this decoding dominates inference time (similar to Gaussian Grouping in Tab. 3).

Image quality evaluation. Our method preserves competitive rendering quality compared to vanilla 3DGS. Detailed PSNR/SSIM/LPIPS results are provided in the appendix.

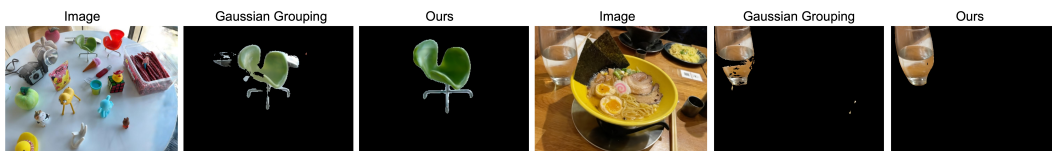


Figure 5: Example of 3D open-vocabulary segmentation on the LERF-Mask dataset.

Table 3: Runtime breakdown (ms per frame).

Methods	Feature Dim	Rendering Time	Decoding Time	Total Time	Speed (FPS)
Gaussian Grouping [4]	16	10.04	12.87	22.91	43.6
ObjectGS [12]	32	12.72	-	12.72	78.6
Ours	2	8.2	-	8.2	121.7

Table 4: Ablation study of dual-opacity in two stages.

Dataset	Method Type	Baseline		Dual-opacity	
		mIoU	mBIoU	mIoU	mBIoU
3DOVS	Oracle	76.1	64.7	97.1	92.0
	Query	76.1	64.7	97.1	92.0
LERF_MASK	Oracle	52.1	45.6	92.4	87.9
	Query	37.8	33.5	90.1	86.4

4.3 Qualitative Result

3D open-vocabulary segmentation. Qualitative examples are shown in Fig. 5. Our method produces clean masks with minimal background noise, especially near object boundaries. Thanks to the independent opacity design, it also handles transparent objects well, such as the glass of water. More visualization results are provided in the appendix. **3D instance segmentation.** We qualitatively evaluate our method on the Replica dataset [23] for instance segmentation. The visualization results are provided in the appendix.

4.4 Ablation Study

In this section, we present ablation studies to analyze the contribution and robustness of our proposed method. Additional ablation studies on the number of sampled objects, training steps, and the hyper-parameter λ_o in Eq. 9 are presented in the appendix.

Dual-opacity and random object loss. We performed a diagnostic ablation to isolate the effect of our dual-opacity formulation. The results are shown in Tab. 4. **Baseline:** standard 3DGS is trained using only the original opacity σ , Gaussian labels are assigned post-hoc via majority voting from SAM2 masks, and object masks are rendered using σ with max-opacity rendering. The proposed **Dual-opacity** setting instead activates σ^* in stage 2 and learns it with the random object loss, enabling identity learning during training. To separate raw mask quality from CLIP retrieval, we report (1) *Oracle mode*, where the ground-truth object ID is picked to render its mask, and (2) *Query mode*, where the object ID is selected via text-CLIP retrieval. Across both 3DOVS and LERF-Mask, the **Dual-opacity** variant yields substantially better mask quality (e.g., 76.1→97.1 mIoU on 3DOVS; 37.8→90.1 on LERF-Mask), demonstrating that learning σ^* is crucial for achieving consistent, view-stable object separation, which the **Baseline** cannot recover even with ideal ID matching; once masks are reliable, retrieval accuracy naturally follows. Since the baseline has only a single opacity, maximum-opacity rendering is the optimal strategy for mask extraction. In contrast, our dual-opacity method applies a 0.5 threshold on σ^* to extract masks.

5 Discussion and Conclusion

We propose *OP2GS*, a dual-opacity Gaussian Splatting framework for efficient open-vocabulary 3D segmentation. By augmenting each Gaussian with an instance opacity σ^* , OP2GS introduces a compact instance occupancy field that decouples visual reconstruction from object-mask rendering. This design enables object-aware primitives with reduced memory and rendering overhead while preserving photorealistic reconstruction. Object-level CLIP embeddings are computed after training from geometry-gated multi-view crops, making semantic attachment modular and independent of per-Gaussian feature decoding. **Limitation.** Like existing approaches [4, 12, 18], our method relies on view-consistent masks generated by 2D segmentation models like SAM or SAM2. **Further improvements.** Because our method assigns a single label to each Gaussian, it is compatible with interactive approaches such as ClickGaussian [17] for user-guided refinement. Our future work will further improve full-scene segmentation accuracy and robustness.

References

- [1] Alexander Kirillov, Eric Mintun, Nikhila Ravi, Hanzi Mao, Chloe Rolland, Laura Gustafson, Tete Xiao, Spencer Whitehead, Alexander C. Berg, Wan-Yen Lo, Piotr Dollar, and Ross Girshick. Segment anything. In *Proceedings of the IEEE/CVF International Conference on Computer Vision (ICCV)*, pages 4015–4026, October 2023.
- [2] Bernhard Kerbl, Georgios Kopanas, Thomas Leimkühler, and George Drettakis. 3d gaussian splatting for real-time radiance field rendering. *ACM Trans. Graph.*, 42(4):139–1, 2023.
- [3] Shijie Zhou, Haoran Chang, Sicheng Jiang, Zhiwen Fan, Zehao Zhu, Dejia Xu, Pradyumna Chari, Suyu You, Zhangyang Wang, and Achuta Kadambi. Feature 3dgs: Supercharging 3d gaussian splatting to enable distilled feature fields. In *Proceedings of the IEEE/CVF Conference on Computer Vision and Pattern Recognition*, pages 21676–21685, 2024.
- [4] Mingqiao Ye, Martin Danelljan, Fisher Yu, and Lei Ke. Gaussian grouping: Segment and edit anything in 3d scenes. In *European Conference on Computer Vision*. Springer, 2024.
- [5] Yanmin Wu, Jiarui Meng, Haijie Li, Chenming Wu, Yahao Shi, Xinhua Cheng, Chen Zhao, Haocheng Feng, Errui Ding, Jingdong Wang, and Jian Zhang. Opegaussian: Towards point-level 3d gaussian-based open vocabulary understanding. In *Advances in Neural Information Processing Systems (NeurIPS)*, 2024.
- [6] Jaehun Bang, Jinhyeok Kim, Minji Kim, Seungheon Jeong, and Kyungdon Joo. Lightsplat: Fast and memory-efficient open-vocabulary 3d scene understanding in five seconds. In *CVPR*, 2026.
- [7] Jiahuan Cheng, Jan-Nico Zaech, Luc Van Gool, and Danda Pani Paudel. Occam’s lgs: An efficient approach for language gaussian splatting. *arXiv preprint arXiv:2412.01807*, 2024.
- [8] Kim Jun-Seong, GeonU Kim, Kim Yu-Ji, Yu-Chiang Frank Wang, Jaesung Choe, and Tae-Hyun Oh. Dr. splat: Directly referring 3d gaussian splatting via direct language embedding registration. In *Proceedings of the Computer Vision and Pattern Recognition Conference*, pages 14137–14146, 2025.
- [9] Tao Lu, Mulin Yu, Linning Xu, Yuanbo Xiangli, Limin Wang, Dahua Lin, and Bo Dai. Scaffold-gs: Structured 3d gaussians for view-adaptive rendering. In *Proceedings of the IEEE/CVF Conference on Computer Vision and Pattern Recognition*, pages 20654–20664, 2024.
- [10] Alec Radford, Jong Wook Kim, Chris Hallacy, Aditya Ramesh, Gabriel Goh, Sandhini Agarwal, Girish Sastry, Amanda Askell, Pamela Mishkin, Jack Clark, et al. Learning transferable visual models from natural language supervision. In *International conference on machine learning*, pages 8748–8763. PMLR, 2021.
- [11] Jiazhong Cen, Jiemin Fang, Chen Yang, Lingxi Xie, Xiaopeng Zhang, Wei Shen, and Qi Tian. Segment any 3d gaussians. In *Proceedings of the AAAI Conference on Artificial Intelligence*, pages 1971–1979, 2025.
- [12] Ruijie Zhu, Mulin Yu, Linning Xu, Lihan Jiang, Yixuan Li, Tianzhu Zhang, Jiangmiao Pang, and Bo Dai. Objectgs: Object-aware scene reconstruction and scene understanding via gaussian splatting. In *Proceedings of the IEEE/CVF International Conference on Computer Vision*, pages 8350–8360, 2025.
- [13] Justin Kerr, Chung Min Kim, Ken Goldberg, Angjoo Kanazawa, and Matthew Tancik. Lurf: Language embedded radiance fields. In *Proceedings of the IEEE/CVF Conference on Computer Vision and Pattern Recognition (CVPR)*, pages 12806–12816, 2023.
- [14] Francis Engelmann, Fabian Manhardt, Michael Niemeyer, Keisuke Tateno, and Federico Tombari. OpenneRF: Open set 3d neural scene segmentation with pixel-wise features and rendered novel views. In *The Twelfth International Conference on Learning Representations*, 2024. URL <https://openreview.net/forum?id=SgjAojPKb3>.
- [15] Minghan Qin, Wanhua Li, Jiawei Zhou, Haoqian Wang, and Hanspeter Pfister. Langsplat: 3d language gaussian splatting. In *Proceedings of the IEEE/CVF Conference on Computer Vision and Pattern Recognition (CVPR)*, pages 23606–23615, 2024.
- [16] Yue Li, Qi Ma, Runyi Yang, Huapeng Li, Mengjiao Ma, Bin Ren, Nikola Popovic, Nicu Sebe, Ender Konukoglu, Theo Gevers, et al. Scenesplat: Gaussian splatting-based scene understanding with vision-language pretraining. In *Proceedings of the IEEE/CVF International Conference on Computer Vision*, pages 4961–4972, 2025.
- [17] Seokhun Choi, Hyeonseop Song, Jaechul Kim, Taehyeong Kim, and Hoseok Do. Click-gaussian: Interactive segmentation to any 3d gaussians. In *ECCV (3)*, pages 289–305, 2024.

- [18] SungMin Jang and Wonjun Kim. Identity-aware language gaussian splatting for open-vocabulary 3d semantic segmentation. In *Proceedings of the IEEE/CVF International Conference on Computer Vision*, pages 20467–20476, 2025.
- [19] Sen Wang, Kunyi Li, Siyun Liang, Elena Alegret, Jing Ma, Nassir Navab, and Stefano Gasperini. Visibility-aware language aggregation for open-vocabulary segmentation in 3d gaussian splatting. *arXiv preprint arXiv:2509.05515*, 2025.
- [20] Juliette Marrie, Romain Ménégaux, Michael Arbel, Diane Larlus, and Julien Mairal. Ludvig: Learning-free uplifting of 2d visual features to gaussian splatting scenes. In *Proceedings of the IEEE/CVF International Conference on Computer Vision*, pages 7440–7450, 2025.
- [21] Jens Piekenbrinck, Christian Schmidt, Alexander Hermans, Narunas Vaskevicius, Timm Linder, and Bastian Leibe. Opensplat3d: Open-vocabulary 3d instance segmentation using gaussian splatting. In *Proceedings of the Computer Vision and Pattern Recognition Conference*, pages 5246–5255, 2025.
- [22] Kunhao Liu, Fangneng Zhan, Jiahui Zhang, Muyu Xu, Yingchen Yu, Abdulmotaleb El Saddik, Christian Theobalt, Eric Xing, and Shijian Lu. Weakly supervised 3d open-vocabulary segmentation. *Advances in Neural Information Processing Systems*, 36:53433–53456, 2023.
- [23] Julian Straub, Thomas Whelan, Lingni Ma, Yufan Chen, Erik Wijmans, Simon Green, Jakob J Engel, Raul Mur-Artal, Carl Ren, Shobhit Verma, et al. The replica dataset: A digital replica of indoor spaces. *CoRR*, abs/1906.05797, 2019.
- [24] Boyi Li, Kilian Q Weinberger, Serge Belongie, Vladlen Koltun, and René Ranftl. Language-driven semantic segmentation. *arXiv preprint arXiv:2201.03546*, 2022.
- [25] Feng Liang, Bichen Wu, Xiaoliang Dai, Kunpeng Li, Yinan Zhao, Hang Zhang, Peizhao Zhang, Peter Vajda, and Diana Marculescu. Open-vocabulary semantic segmentation with mask-adapted clip. In *Proceedings of the IEEE/CVF conference on computer vision and pattern recognition*, pages 7061–7070, 2023.
- [26] Rohan Chacko, Nicolai Häni, Eldar Khaliullin, Lin Sun, and Douglas Lee. Lifting by gaussians: A simple, fast and flexible method for 3d instance segmentation. In *2025 IEEE/CVF Winter Conference on Applications of Computer Vision (WACV)*, pages 3497–3507. IEEE, 2025.
- [27] Ho Kei Cheng, Seoung Wug Oh, Brian Price, Alexander Schwing, and Joon-Young Lee. Tracking anything with decoupled video segmentation. In *Proceedings of the IEEE/CVF International Conference on Computer Vision*, pages 1316–1326, 2023.
- [28] Jiazhong Cen, Zanwei Zhou, Jiemin Fang, Wei Shen, Lingxi Xie, Dongsheng Jiang, Xiaopeng Zhang, Qi Tian, et al. Segment anything in 3d with nerfs. *Advances in Neural Information Processing Systems*, 36: 25971–25990, 2023.
- [29] google. slang-gaussian-rasterization. <https://github.com/google/slang-gaussian-rasterization>, 2024.
- [30] Binbin Huang, Zehao Yu, Anpei Chen, Andreas Geiger, and Shenghua Gao. 2d gaussian splatting for geometrically accurate radiance fields. In *ACM SIGGRAPH 2024 conference papers*, pages 1–11, 2024.

A Technical appendices and appendix

A.1 The Process of Open-vocabulary Querying

As shown in Fig. 6, we first render the object masks in N training views and crop the object regions. Then, we feed these cropped images into the CLIP image encoder to obtain the features. Finally, we average the features from N views to get the final object embedding.

A.2 More Ablation Study Results

Number of random objects during training. As shown in Tab. 1, even $M = 1$ achieves strong performance, where only the gradients related to a single object are updated, enabling lightweight training. Increasing M improves stability, but the benefit becomes marginal beyond $M = 2$. We set $M = 3$ in all experiments to balance efficiency and accuracy.

Loss weight of instance opacity supervision. We conduct ablation studies on the loss weight of object opacity supervision λ_o in Tab. 2. From the results, even when λ_o ranges from 0.01 to 1, our method achieves good

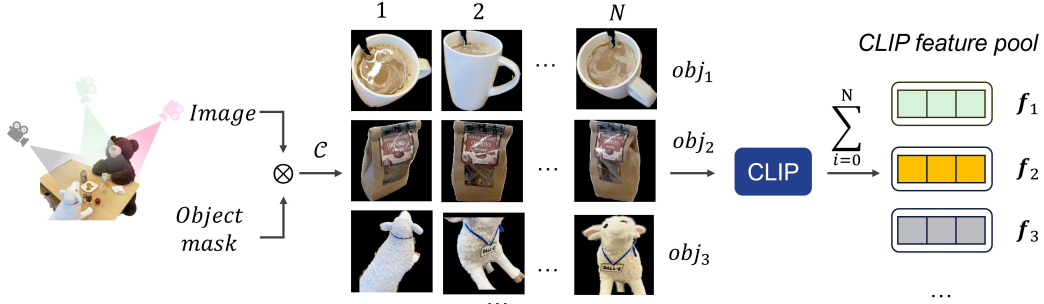


Figure 6: Object embedding aggregation. We choose N training views to render object masks. The cropped object regions are fed into the CLIP image encoder, and the final object embedding is obtained by averaging features from N views.

Table 1: Ablation study on the number of random objects. M denotes the number of objects updated during training.

M	3DOVS		LERF-Mask	
	mIoU	mBIOU	mIoU	mBIOU
$M = 1$	96.9	91.4	87.3	83.4
$M = 2$	97.1	91.7	89.0	85.0
$M = 3$	97.1	92.0	90.1	86.4

performance on both datasets. For complex scenes like LERF-Mask, a too small or too large λ_o slightly decreases the performance. For simple scenes like 3DOVS, the performance is relatively stable under different λ_o values.

Training steps. We also conduct an ablation study on the starting step of the second-stage training. The results are shown in Tab. 3. Our default setting starts the second-stage training at 20,000 steps (30,000 steps in total). At the start of the second stage, we perform majority voting for all Gaussians to determine their object labels. When starting voting too early at step 10,000, the original Gaussian primitives are not well-optimized. Since our σ^* is initialized by the original opacity σ , early voting may not lead to the best results. In contrast, starting after step 20,000, we observe that the performance is relatively stable. An exception arises at step 15,000 on the LERF-Mask dataset, where the result is significantly lower than in other settings. This drop occurs because, in the original 3DGS training schedule, the opacity is reset to zero to remove unimportant floaters. After this reset, important Gaussians recover to normal opacity values after several training steps. Therefore, when applying our method, it is preferable to avoid immediately starting the second stage following the opacity reset.

A.3 Qualitative Results

A.3.1 Qualitative Results of Instance Segmentation

We also adapt our method to the Replica dataset [23] for instance segmentation. The results are shown in Fig. 7. Compared with the majority-voting baseline in Fig. 1, these results show that our method suppresses mislabeled Gaussian points, including floaters and edge artifacts, resulting in cleaner and more accurate instance masks.

A.3.2 Visualization of Different Methods

As shown in Fig. 8, we provide additional visualization results of different methods on both datasets. Our method preserves object details, such as the camera strap, and produces cleaner masks around objects such as the green chair and rubber duck in Fig. 8.

A.3.3 Visualization of Training Process and Different Thresholds

To show the training process of the additional instance opacity σ^* , we visualize the rendered mask in both the early and final stages. The results are shown in Fig. 9.

Since opacity values range from 0 to 1, we set the threshold τ to 0.5 for all object classes in the experiments. To further demonstrate the robustness of our rendered instance occupancy maps, we present the effects of different thresholds for generating binary masks, as shown in Fig. 10. As illustrated in Fig. 10, our method robustly segments the target object across different thresholds. With a lower threshold such as $\tau = 0.2$, the segmented

Table 2: Ablation study on hyper-parameter λ_o .

Objects	3DOVS		LERF-Mask	
	mIoU	mBIoU	mIoU	mBIoU
$\lambda_o = 0.01$	97.0	91.2	89.1	84.8
$\lambda_o = 0.03$	97.0	91.4	89.1	84.9
$\lambda_o = 0.1$	97.1	92.0	90.1	86.4
$\lambda_o = 0.3$	97.1	91.8	89.8	84.6
$\lambda_o = 1$	97.1	92.0	89.0	84.8

Table 3: Ablation study on the starting step of the second-stage training.

Start step	3DOVS		LERF-Mask	
	mIoU	mBIoU	mIoU	mBIoU
10,000	97.0	91.5	86.8	81.7
15,000	97.0	91.7	82.9	78.3
16,000	97.1	91.8	88.1	83.7
20,000	97.1	92.0	90.1	86.4
25,000	97.1	92.0	90.4	86.5

masks do not expand excessively, indicating effective suppression of mislabeled Gaussians. Even with a high threshold such as $\tau = 0.8$, the segmented masks show only minor holes compared to the ground truth.

A.4 Initialization details

Our method follows a two-stage training strategy. In the first stage, we optimize the standard 3DGS parameters with the reconstruction loss. During this stage, Gaussian densification increases the number of primitives until a predefined step, after which the point growth stops and the reconstruction loss approaches convergence. We then initialize the scalar object label l for each densified Gaussian and start the second stage, where the additional instance opacity σ^* is optimized by the proposed instance learning objective.

For label initialization, we first obtain per-view instance masks using an off-the-shelf SAM2 model. For each Gaussian j with center μ_j , we project it onto each training view and read the instance ID at the projected pixel. The final scalar label is determined by majority voting across views. Previous methods often combine SAM with tracking methods such as DEVA to obtain view-consistent masks. In contrast, we directly use SAM2 to obtain view-consistent masks, simplifying the pseudo-label pipeline.

A.5 Pseudo-label generation and supervision

How is SAM2 used to extract pseudo-label masks? We use off-the-shelf SAM2 with automatically generated uniform click prompts to obtain pseudo masks. For example, 32 click prompts can be uniformly distributed across the first image of a sequence. Once the masks are obtained from the first image, they are automatically tracked in the subsequent frames.

To supervise the training of 3D Gaussian Splatting, previous methods use SAM [1] to obtain per-view masks. Tracking-based methods such as DEVA [27] are then used alongside SAM to ensure mask consistency across different views within a scene. LangSplat [15] uses three layers of SAM masks (small, middle, and large), while OpenGaussian [5] only uses the large layer masks for supervision. Gaussian Grouping [4] additionally suppresses the small masks extracted from SAM.

SAM2 expanded segmentation to video sequences, eliminating the need for outsourced tracking methods. We use SAM2 as our primary supervision method. To provide a comparative analysis, we also test the performance of SAM+DEVA as the pseudo-label, following Gaussian Grouping [4]. The result is shown in Tab. 4 and Tab. 5. As presented in Tab. 1, on the 3DOVS [22] dataset, using SAM2 or SAM+DEVA makes almost no difference, since there are only a few objects to track. For more complex scenes in the LERF-Mask [13] dataset, SAM2 provides more robust segmentation masks, resulting in better performance than SAM+DEVA, as shown in Tab. 5. Nevertheless, our method achieves good results under both pseudo-label masks.

A.6 Majority voting

When we start the second stage of training, we need to initialize the object label for each Gaussian. We get the label through projection and majority voting. The details below describe the process of majority voting.

Given the input images $\{I_i\}$, we generate corresponding ID maps $\{L_i\}$:

$$\{L_i\} = \text{SAM2}(\{I_i\}, \text{Prompts}), \quad (13)$$

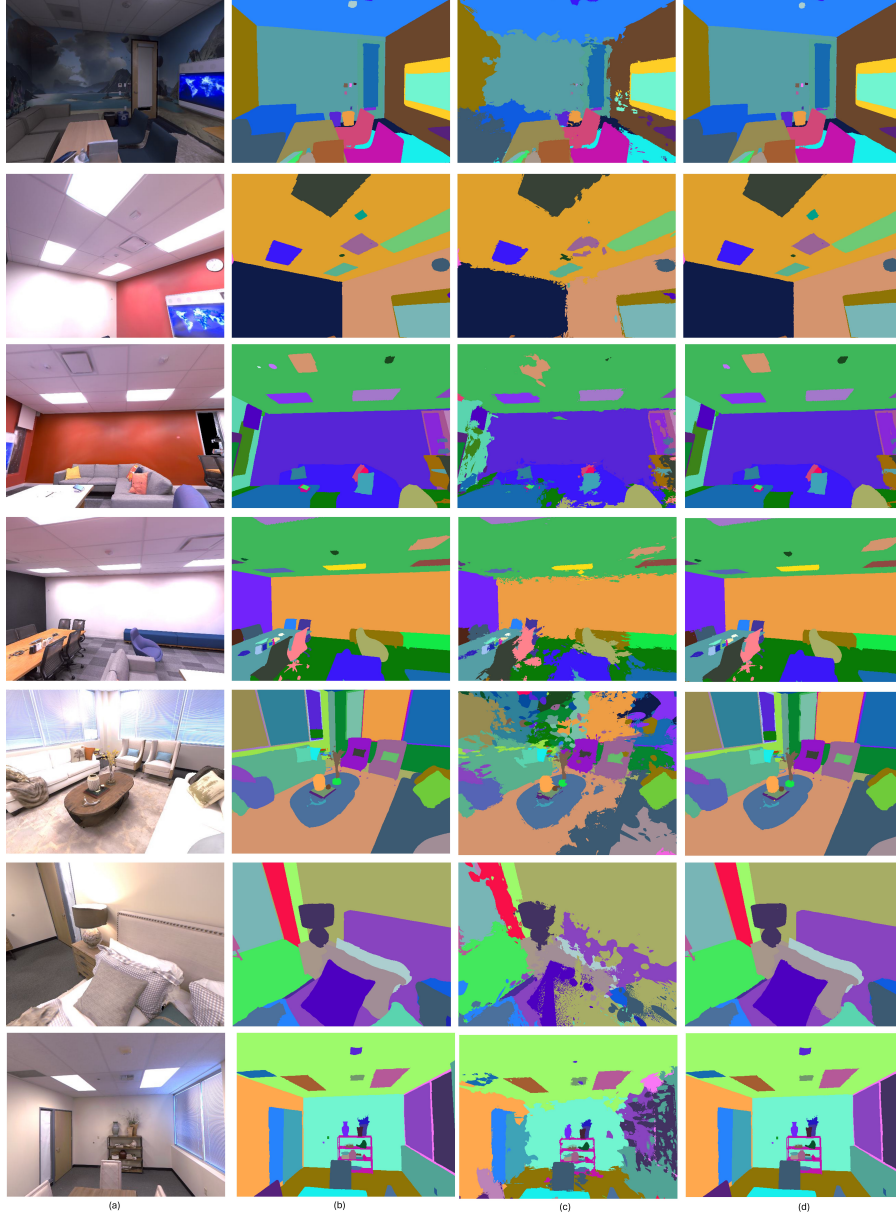


Figure 7: Qualitative instance segmentation results on the Replica dataset. (a) Input image. (b) 2D pseudo-label mask. (c) Rendered instance mask obtained by selecting the Gaussian with the largest rendering weight $\alpha_i T_i$ along each ray after majority voting and depth culling. (d) Rendered instance mask after applying our proposed loss.

where L_i stores pixel-wise instance IDs, and background or unlabeled pixels are set to 0. Suppose the scene contains C objects; we index the IDs as 0 for background and $1, \dots, C$ for objects.

For each Gaussian j with center μ_j , we project it onto view i using the camera pose C_i (projection π_i) and read the ID value at the projected pixel. The final label is determined by majority voting:

$$l_j = \arg \max_{k \in \{0, \dots, C\}} \sum_{i \in \mathcal{V}_j} \mathbf{1}[L_i(\pi_i(\mu_j)) = k], \quad (14)$$

where \mathcal{V}_j denotes the set of views in which Gaussian j is visible, and $k = 0$ indicates background while $k = 1, \dots, C$ indicate object IDs.



Figure 8: Open-vocabulary 3D segmentation results of different methods on the LERF-Mask dataset. (a) Input image. (b) Ground-truth mask. (c) Gaussian Grouping. (d) ObjectGS. (e) Ours.

Table 4: Open-vocabulary 3D segmentation results. We report mIoU (%) on 3DOVS dataset following prior work.

Method	Pseudo-label	bed	bench	room	lawn	sofa	MEAN
ObjectGS [12]	SAM + DEVA	98.0	96.4	95.1	97.2	95.4	96.4
Ours	SAM + DEVA	97.5	96.3	97.3	97.5	96.4	97.0
Ours	SAM2	97.5	96.3	97.4	97.7	96.4	97.1

A.7 Implementation Details

All experiments were conducted using the PyTorch framework and custom CUDA kernels, built upon the Slang 3DGS framework [29]. Our model is trained in an end-to-end manner on a single NVIDIA RTX A4000 GPU with 16GB of memory. Each scene is trained for 30,000 iterations, consistent with previous methods. In all experiments, the loss weight λ_o is set to 0.1, while λ_{SSIM} is set to 0.2, with the second stage commencing from 20,000 iterations.

When extracting CLIP features for each object, we use “ViT-B-16” as the base image encoder. First, we render the object in each visible training view and select the top five views with the largest visible areas. We then resize the cropped object regions to 224×224 and feed them into the CLIP image encoder to obtain image features. Finally, we average these feature vectors to obtain the final object embedding.

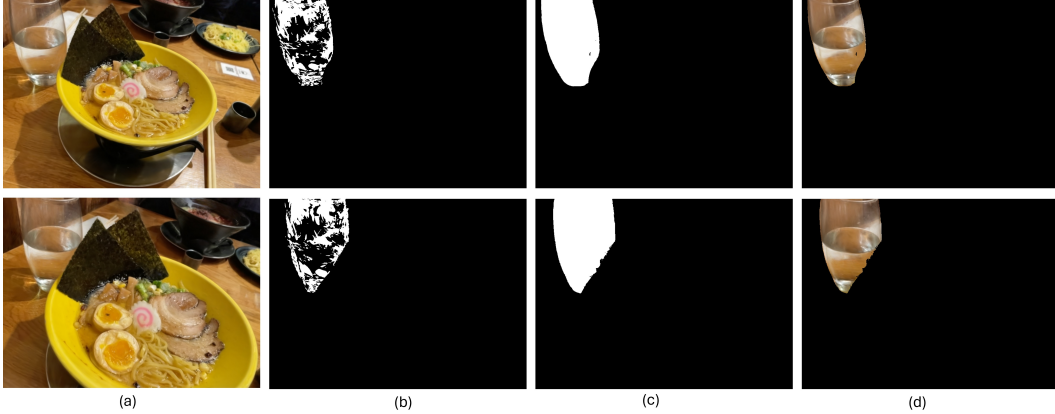


Figure 9: (a) Ground-truth image. (b) Early stage rendered mask. (c) Final rendered mask. (d) Final masked object image.

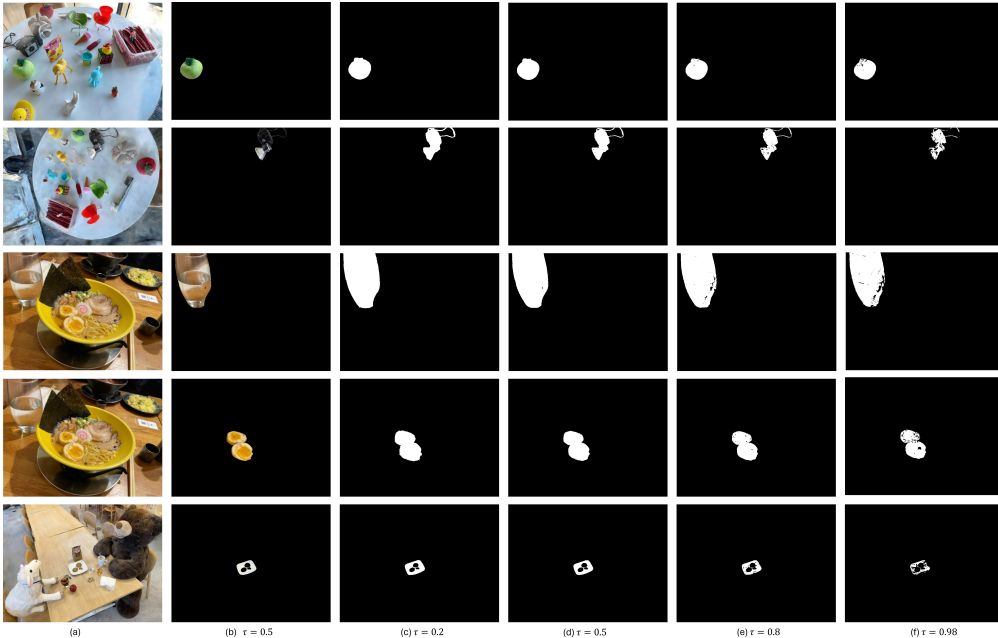


Figure 10: Examples of rendered instance masks under different thresholds τ . (a) Ground-truth image. (b) Masked image at $\tau = 0.5$. (c–f) Rendered binary masks at different thresholds.

A.8 Image Quality Evaluation

To verify that our additional opacity σ^* does not compromise rendering quality, we evaluate novel view synthesis on the LERF-Mask [13] dataset following the same protocol as ILGS [18]. As shown in Tab. 6, our method maintains competitive rendering quality compared to vanilla 3DGS [2], demonstrating that our method preserves photorealistic rendering while enabling fast segmentation.

We compare the image quality of our method with Gaussian Grouping [4]. As shown in Fig. 11, our method produces fewer artifacts and better preserves details in the rendered images.

A.9 More Results on 3DOVS Dataset

We evaluate our method on five additional scenes from the 3DOVS dataset (Tab. 7). In these five scenes, we only fine-tune the prompt from "desktop" to "desk" for the scene "covered_desk". Notably, our method demonstrates strong performance on these scenes, achieving an impressive average mIoU of 97.7%.

Table 5: Open-vocabulary segmentation results on the LERF-Mask dataset. We follow Gaussian Grouping [4] to evaluate the method.

Model	Pseudo-label	figurines		ramen		teatime	
		mIoU	mBIoU	mIoU	mBIoU	mIoU	mBIoU
ObjectGS[12]	SAM + DEVA	88.2	85.2	88.0	79.9	88.9	88.6
Ours	SAM + DEVA	91.2	87.5	90.0	82.3	86.8	85.1
Ours	SAM2	92.3	89.1	91.0	84.6	87.0	85.4

Table 6: Performance comparisons of novel view rendering on the LERF-Mask dataset.

Methods	PSNR \uparrow	SSIM \uparrow	LPIPS \downarrow
3DGS[2]	25.870	0.867	0.211
Gaussian Grouping[4]	25.710	0.852	0.235
ILGS[18]	26.108	0.868	0.210
Ours	25.210	0.890	0.187

A.10 Compatibility and Extensibility

Our method is highly compatible with existing Gaussian Splatting frameworks. It relies only on the alpha rendering process and can be readily extended to 2DGS [30]. It can also be integrated into other 3D Gaussian Splatting methods that employ densification, such as ScaffoldGS [9]. The random object loss is applied after densification, allowing incorporation as an additional training stage in these frameworks.

We focus on image-reconstructed 3DGS scenes rather than RGB-D point-initialized ScanNet evaluation, because OP2GS targets object-mask ambiguity arising from standard 3DGS optimization with soft alpha compositing and densification. RGB-D point initialization converts 3DGS into a more surface-aligned point-labeling setting, which reduces the soft-opacity artifacts and floater ambiguities that our dual-opacity representation is designed to address. Therefore, our evaluation emphasizes primitive-level label consistency under standard 3DGS rendering. Unlike methods with implicit identity features [4, 15, 18], which obtain 3D points through rendered classification masks, multi-view lifting, and post-processing (e.g., computing the convex hull of lifted 3D points), our approach assigns each Gaussian a single label. This explicit labeling enables direct 3D instance operations (such as selection, removal, and inpainting).

For object embedding extraction, we select the N views with the largest visible object areas. This embedding could also be improved by using virtual views rendered from the trained Gaussian Splatting model. This approach may yield more robust object features and, furthermore, could expand to more complex text query scenarios.

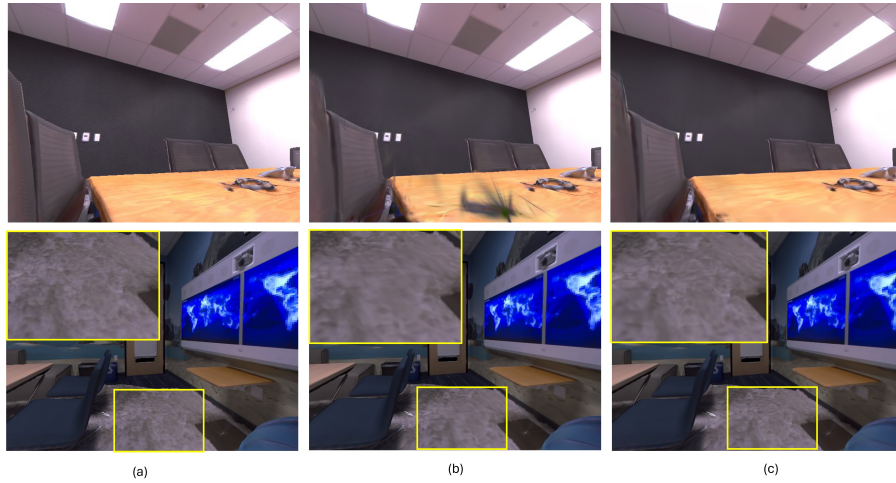


Figure 11: Qualitative rendering results on the Replica dataset. (a) Ground-truth image. (b) Gaussian Grouping rendered image. (c) Ours.

Table 7: Open-vocabulary 3D segmentation results. We report mIoU (%) on 3DOVS dataset following prior work.

Method	blue sofa	covered desk	office desk	snacks	table	MEAN
Ours	97.7	97.1	98.9	98.4	96.6	97.7